Progress In Electromagnetics Research C, Vol. 83, 179–194, 2018

Design and Analysis of a Novel Low Loss Ultra-Wideband Coplanar Waveguide (CPW) to Coplanar Strips (CPS) Transition for Tapered Slot Antennas (TSA) in Ground Penetrating Radar (GPR) Application

Mohammed M. Mohanna[1, *], Esmat A. Abdallah[2], Hadia M. Elhennawy[3], and Magdy A. Attia[4]

Abstract—A novel ultra-wideband CPW to CPS transition for TSA in landmine detection by GPR system is proposed. The structure is constructed on a $140 \times 140\,\text{mm}^2$ FR4 dielectric substrate. It is composed of 2 sections. The first is nonuniform tapered asymmetric coplanar waveguide (TACPW), and the second section is nonuniform Tapered Asymmetric Coplanar Strips (TACPS). Electromagnetic Band Gap (EBG) structure of coplanar circular patches exists near the transition open slot and aligned with the outer edge of the CPW ground to act as a capacitive loading. The design of the proposed transition is given in very simple four design steps. The CPW to CPS transition is analyzed theoretically and experimentally. To characterize this transition, back to back transition is constructed; besides, the equivalent-circuit model that consists of nonuniform transmission lines is established. The equivalent circuit is constructed by dividing both sections TACPW and TACPS into 35 sections and using $ABCD$ parameters to characterize each section, and conversion to S-parameters is done using MATLAB Program. The selection criterion of the section length is to maintain a linear change in the characteristic impedance with the distance. The results based on equivalent-circuit model, CST simulation (CST studio ver. 15), and measurements are compared. Several parameters are studied through simulations and experiments which are used to derive some design guidelines. The operational bandwidth for the CPW to CPS transition covers from 0 (DC) to almost 10 GHz with minimum return loss reaches -50 dB. For the GPR application (landmine detection) which extends from 0.4 to 3 GHz, the insertion loss of the proposed transition reaches almost -0.5 dB which satisfies the design requirements. The back to back transition performance was simulated and measured. Good agreement is found between numerical and experimental results especially for the GPR ranges of frequencies. The proposed transition has the advantages of compact size, ultra-wide bandwidth, and straightforward design procedure.

1. INTRODUCTION

Transition structures are employed to match between two different types of transmission lines to achieve impedance matching and field matching [1]. CPW and CPS are used heavily in microwave integrated circuits and microwave components such as mixers and antennas. Readily available transmission lines such as coaxial cables are inexpensive and have $50\,\Omega$ characteristic impedance. When these cables are used to feed balanced structure such as Tapered Slot Antennas or Archimedean Spiral which are used in GPR antenna, a lot of problems happen. Firstly, there is impedance mismatch, because the coaxial cables have $50\,\Omega$ characteristic impedance, while the input impedance of Tapered Slot Antennas (TSA) and Archimedean Spiral is larger than $50\,\Omega$. This mismatch increases reflection coefficient significantly,

Received 20 March 2018, Accepted 12 April 2018, Scheduled 23 April 2018
* Corresponding author: Mohammed Mahmoud Mohanna (mohanna_2085@hotmail.com).
[1] Ministry of Electricity & Renewable Energy, Abbassia, Cairo, Egypt. [2] Electronics Research Institute, Dokki, Giza, Egypt. [3] Faculty of Engineering, Ain Shams University, Cairo, Egypt. [4] National Research Institute of Astronomy and Geophysics, Egypt.

making the feed unacceptable. Secondly, the coaxial cables have unbalanced structure, and the TSA is a balanced structure. Finally, to fully utilize the advantages of these uniplanar transmission lines, implementation of wide-band and low-loss transitions between CPW and CPS is essential [2].

There are several types of transitions that have been suggested with various degrees of success. The coplanar versions of the traditional Merchand balun is the best known transition, and it uses quarter wavelength segments [3]. This transition has band-pass characteristics with acceptable bandwidths, which is limited by the resonant structures. Double Y-balun in [4] with four resonant stubs is used to achieve a relatively wide bandpass with a compact design. The bandwidth is increased, but small etched gap sizes are required to operate effectively. Asymmetric CPW structure can be used to achieve this transition and transform from unbalanced to balanced conditions [5, 6]. The capacitive loading in the CPW affects widening bandwidth and enhancing power capabilities of the CPW, i.e., enhance the insertion loss of the line [7]. Besides, the modeling and analysis of CPW to CPS transition are done in [8, 9] using $ABCD$ parameters for equivalent circuit model.

The paper is organized as follows. Section 2 presents the final CPW to CPS transition geometry, while Section 3 introduces the proposed CPW to CPS transition design steps: Designing a simple asymmetric CPW with different ground lengths, designing CPW-CPS transition of both linear tapered profile and exponential tapering and the comparison between them, and studying the effect of each design step on return loss and insertion loss in order to reach the optimum design parameters. A comparison between simulation and measured data is done. Section 4 gives the equivalent circuit model using $ABCD$ parameters and analysis of transition, and Section 5 gives the conclusion.

2. CPW TO CPS TRANSITION GEOMETRY

Figure 1 shows the configuration of the proposed CPW to CPS transition with low loss and ultra-wideband. The substrate thickness $h = 1.5\,\text{mm}$, relative dielectric constant $= 4.65$ and $\tan\delta = 0.03$. The structure is composed of 2 sections of nonuniform tapered asymmetric coplanar waveguide (TACPW) and nonuniform Tapered Asymmetric Coplanar Strips (TACPS). For the 1st section TACPW, g_1 and g_2 are the right- and left-hand side ground widths of the CPW, respectively, while W_c is central strip width. S_1 and S_2 are the right- and left-hand side slot widths of the CPW, respectively. The tapering profile of CPW is exponential in the central strip in addition to a part of circle with radius R_1. The 2nd section TACPS is continuing with the same tapering profile as CPW. EBG circular patches are

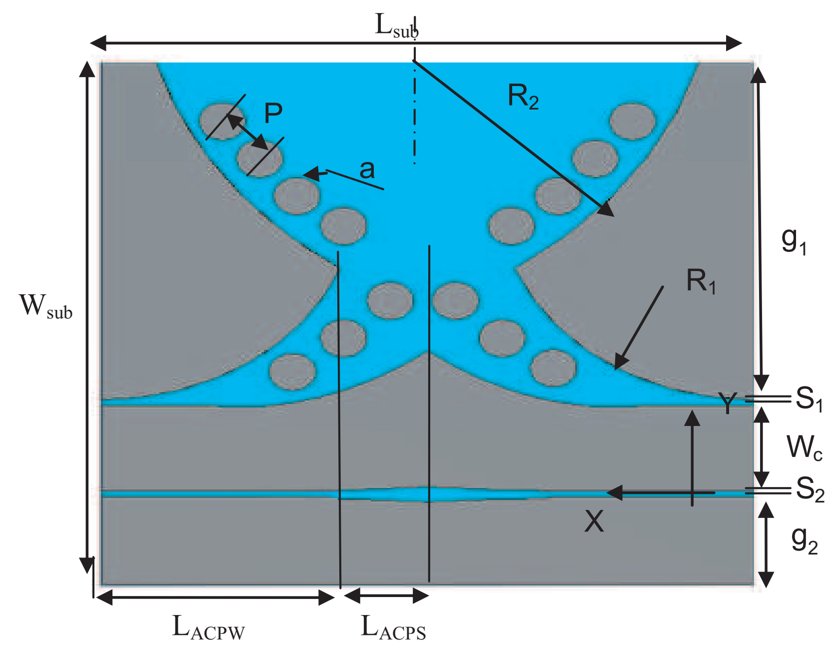

Figure 1. Geometry of the back to back CPW to CPS transition with EBG structure.

Table 1. The proposed CPW to CPS transition dimension (all dimensions in mm).

CPW to CPS Transition												
W_{sub}	L_{sub}	g_1	S_1	W_c	S_2	g_2	R_1	R_2	L_{ACPW}	L_{ACPS}	P	a
14	14	91.2	2.	23.3	2.	20.8	44	81	52	18	26	5
Outer Exponential Rate 1: $\mathbf{2455{*}e^{0.03{*}X^2}}$												

aligned with the outer part of CPW, and CPS acts as a capacitive load with radius "a" and periodicity "P". All simulations are performed using CST ver. 15. All the CPW to CPS transition dimensions are shown in Table 1. In the next section, the transition design steps will be discussed.

3. PROPOSED CPW-CPS TRANSITION DESIGN STEPS AND DISCUSSION

The lack of a proven design procedure of adjustable transition parameters mentioned in Section 2 leads to the development of the design methodology detailed below. The proposed design methodology serves as a guide to establish a starting point that can be made to optimize CPW-CPS transition performance as shown in Fig. 1. Selecting a substrate material is entirely dependent on operational bandwidth and budget. So, we select FR-4 substrate for commercially low cost. The design steps are as follows:

A. Designing a simple asymmetric CPW with different ground lengths (see Fig. 2(a)).
B. Designing asymmetric CPW-CPS transition of linear tapered profile (see Fig. 2(b)).
C. Designing asymmetric CPW-CPS transition of exponential tapered profile (see Fig. 2(c)).
D. Studying the effect of the EBG circular patch capacitive loading on the transition performance.

Figure 2 shows the change in the transition geometry during design steps.

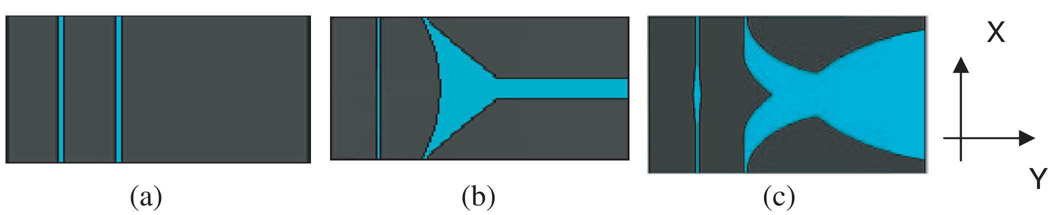

Figure 2. The changes in the CPW to CPS transition geometry during design steps. (a) The Asymmetric CPW. (b) The Asymmetric back to back transition of linear tapered profile. (c) The Asymmetric back to back transition of exponential tapered profile.

The detailed design steps are discussed as follows.

3.1. Designing Asymmetric CPW with Different Ground Length

Figure 3 shows the asymmetric CPW with different ground widths. It is required to design CPW line with 50 Ω characteristic impedance, and to calculate the corresponding geometric parameters g_1, g_2, S_1, S_2 and W_c.

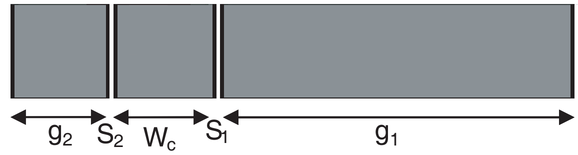

Figure 3. The asymmetric CPW with different ground length.

3.1.1. Design Assumptions and Calculation

For CPW the characteristic impedance is determined by the ratio of centre strip width W_c to gap width (assume firstly), which makes an infinite range of W_c and S values resulting in a specific impedance requirement. In order to calculate the geometric parameters S and W_c, assumptions will be made as follows:

1. Assume that the required CPW will be used in CPW to CPS transition to feed GPR antenna of tapered slot type to detect landmine with ultra-wide bandwidth, and it starts operation from $f_{\min} = 0.4\,\text{GHz}$ to $f_{\max} = 3\,\text{GHz}$. So, the antenna dimension will be in the range of $W_{\text{subtotal}} = 350\,\text{mm}$ and $L_{\text{subtotal}} = 350\,\text{mm}$ [10, 11].
2. Let us begin with the dimensions required for the CPW to CPS transition around 20% of the total antenna dimension calculated in assumption No. 1. The ratio of radiating element dimension to feeding element dimension increases. The antenna gain will be improved and the insertion loss decreased. The assumption of 20% is obtained by roughly reviewing the published papers [2, 12], and it is found that this ratio is (20%–50%). We choose the lower limit for the reasons mentioned above, so $W_{\text{transition.}} = 14\,\text{mm}$ and $L_{\text{transition.}} = 70\,\text{mm}$.
3. Assume using asymmetric CPW with wide ground in the right-hand side and narrow in the left-hand side ground, such that there will be more parameters to achieve impedance matching as shown in Fig. 2(a) and Fig. 3.

Let initial values $g_1 = 90\,\text{mm}$, g_2 =22mm and $S_2 = 2.6\,\text{mm}$. By substituting in the equations of asymmetric CPW in [10, 11] and studying the effect of W_c and S_1 changes on value of characteristic impedance, one can obtain Fig. 4. It can be shown that as S_1 decreases and W_c increases, **Zo** decreases significantly.

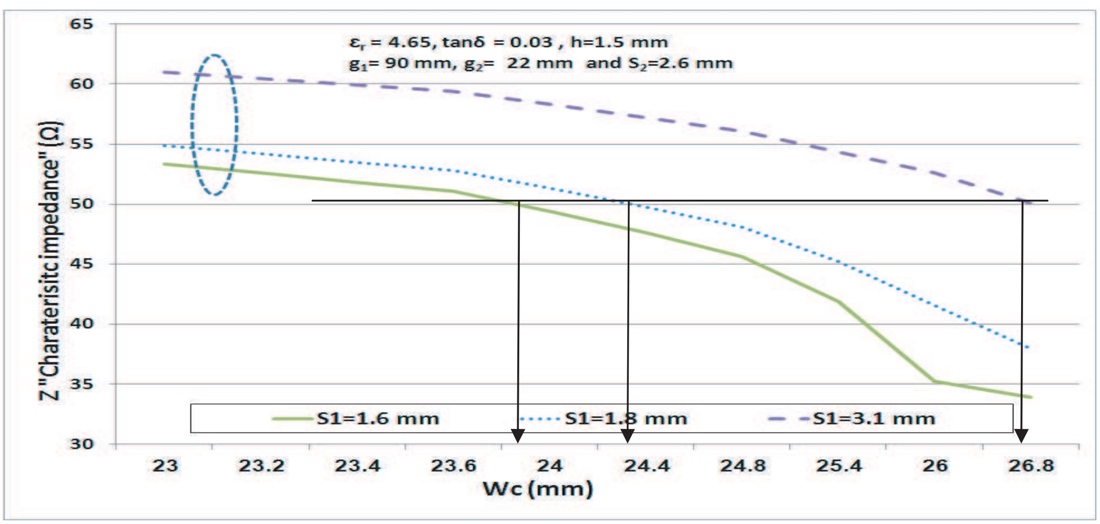

Figure 4. Variation of characteristic impedance Z_o with central strip width W_c.

The sum of all dimension parameters $W_{\text{transition}} = g_1 + g_2 + S_1 + S_2 + W_c = 140\,\text{mm}$.

From Fig. 4, the suitable value of W_c is 23.8 mm and $S_1 = 1.6\,\text{mm}$ that achieve the boundary condition. Checking on the value of g_1 as shown in Fig. 5, one finds that as g_1 increases, the value of the impedance decreases.

Table 2. The final values for the geometrical parameters.

Geometric parameters	g_1	g_2	S_1	S_2	W_c
Final values	90	22	1.6	2.6	23.8

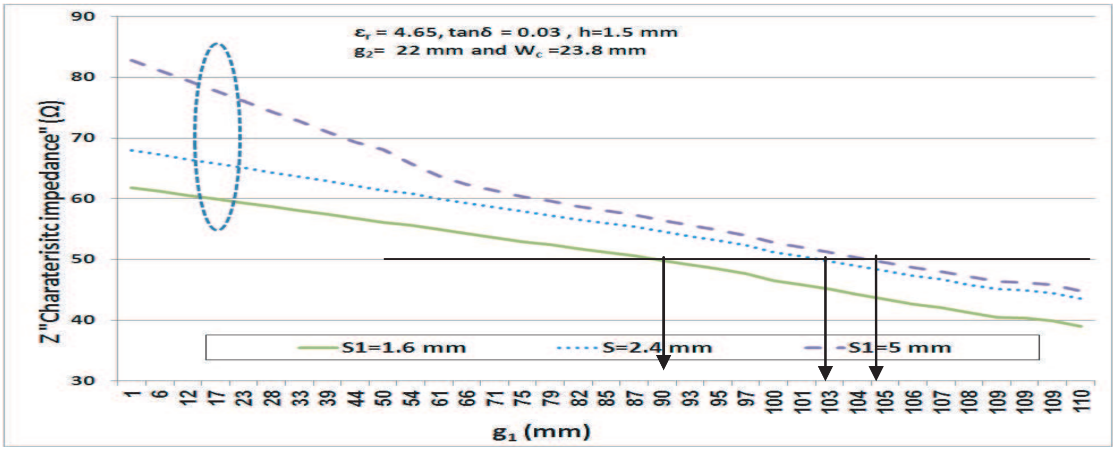

Figure 5. Variation of characteristic impedance Z_o with ground width g_1.

Table 2 shows the final geometric parameter values. A MATLAB program has been constructed to calculate these parameters.

3.2. Designing Asymmetric CPW-CPS Transition of Linear Tapered Profile

It is required to match between slot line antenna with input impedance 100 Ω and coaxial line with 50 Ω characteristic impedance (or CPW = 50 Ω). $g_1 = 90$ mm, $W_c = 23.8$ mm, $S_1 = 1.6$ mm, $g_2 = 22$ mm and $S_2 = 2.6$ mm will be considered as the initial values which are obtained from a previous design of CPW.

It is proposed that the CPW characteristic impedance will change from 50 ohm to 80 ohm and continue with the CPS section until reaches 100 ohm for matching requirements as shown in Fig. 6(a).

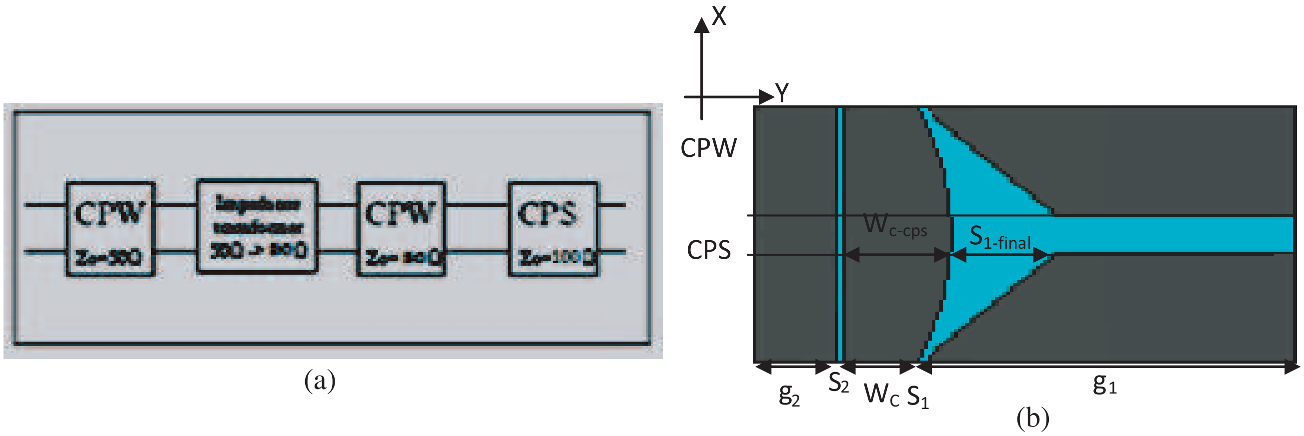

Figure 6. (a) CPW to CPS transition structure steps. (b) Back to back CPW to CPS transition structure of linear tapering.

For Linear tapering with L = tapered line length, Z_1 = input impedance of T.L., Z_2 = input impedance of antenna, and x = length of incremental section [14]

$$Z_o(x) = Z_1 * [1 + \left(\frac{Z_2}{Z_1} - 1\right) * \frac{x}{L}] \tag{1}$$

$Z_1 = 50\,\Omega$ and $Z_2 = 80\,\Omega$.

Assume $L = 70$ mm and $Z_2 = 80\,\Omega$, so, we can calculate $Z_o(x)$ at every incremental change from $x = 0$ to L. The changes of the values of linear tapered characteristic impedance are shown in Fig. 7.

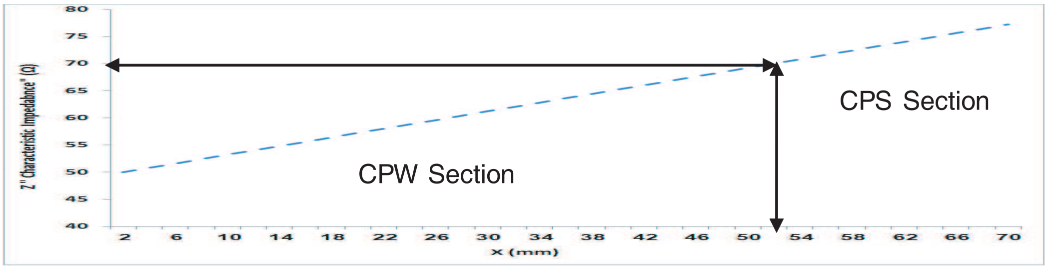

Figure 7. Variation of characteristic impedance versus X (mm) in CPW to CPS transition.

Use the design equation for CPW section in [10, 13] and for the CPS section in [10] to calculate the value of the parameters, shown in Fig. 6(b). Substituting the calculated values of the characteristic impedance in Eq. (1) into ACPW design equations in [13], a MATLAB program is developed to calculate the dimension parameters (S_1, S_2, g_1, g_2, W_c) corresponding to the CPW tapered line variation from $x = 0$ to $x = L$ and started with the values of CPW parameters shown in Table 2. After calculating the dimensional parameters for the CPW section as in [13] using the optimization MATLAB program, it is found that the dimensional parameters S_1, S_2, g_1, g_2, W_c are changed as shown in Fig. 7 which also has linear change for S_1, g_1 and W_c.

Designing the CPS part is done using the equations in [14] till the ACPS matches between the antenna and the CPW section. So, the CPS will continue on the same tapering of CPW, and its calculated dimension parameter is shown in Fig. 8. So, $W_{\text{C}-\text{CPS}} = W_{\text{C}-\text{CPW}} = 31\,\text{mm}$ and $g_2 = 2\,\text{mm}$ and $S_2 = 26\,\text{mm}$ at the same time for the CPW section at the input of the CPS $S_{1\text{final}} = 24\,\text{mm}$ as shown in Fig. 8.

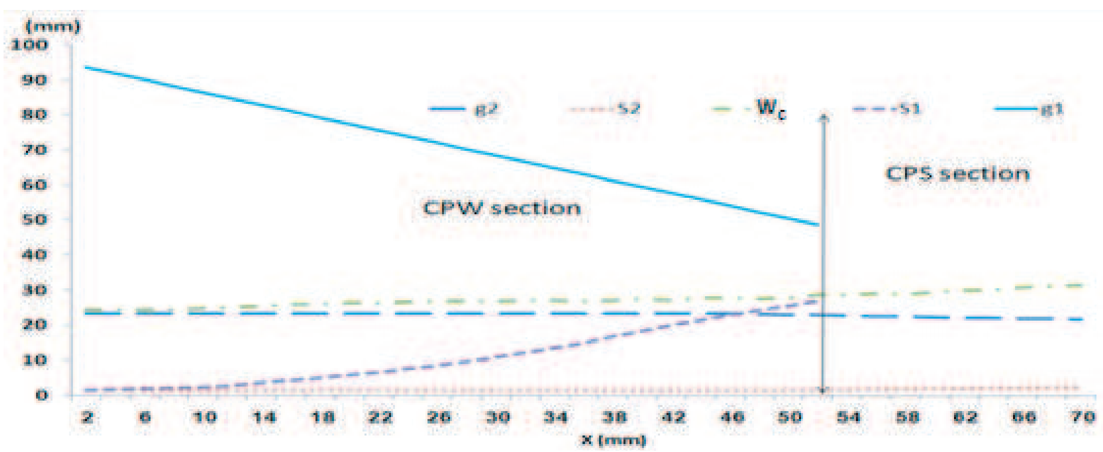

Figure 8. The changes of CPW-CPS transition parameters against transition length.

Back to back CPW to CPS transition is simulated using CST ver. 15, and the bandwidth is found around 1.5 GHz the operating frequencies (1 GHz–2.5 GHz) and the insertion losses $S_{21} = 4\,\text{dB}$.

As shown in Fig. 7, the required length for the CPW section to match 100 ohm CPS will be more than 70 mm, i.e., **the line is lengthy, and the cost is high**.

3.3. Designing Asymmetric CPW-CPS Transition of Exponential Tapered Profile

To design the proposed CPW-to-CPS transition shown in Fig. 9, we will repeat the same procedures stated in Section 3.2. The changes of characteristic impedance of CPW section against length is shown in Fig. 10, while the changes of geometric parameters versus transition length are shown in Fig. 11.

It can be shown from Fig. 1 and Fig. 11 that the required length to achieve the transition from

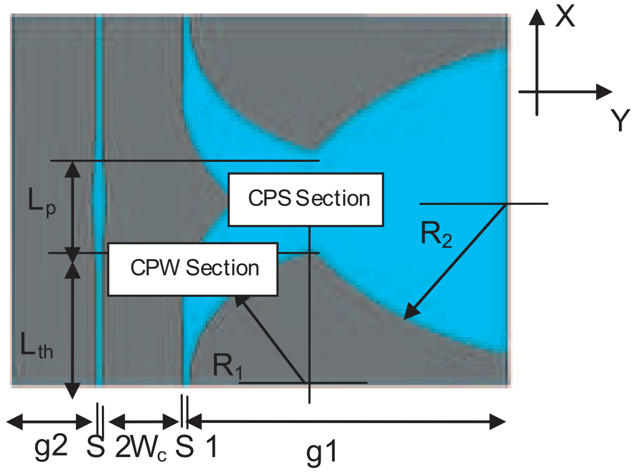

Figure 9. The proposed CPW to CPS transition.

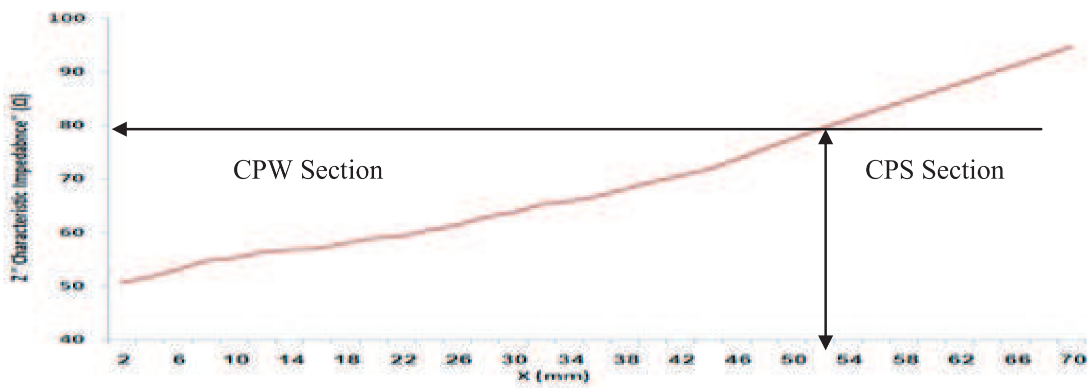

Figure 10. Variation of characteristic impedance versus CPW and CPS section lengths.

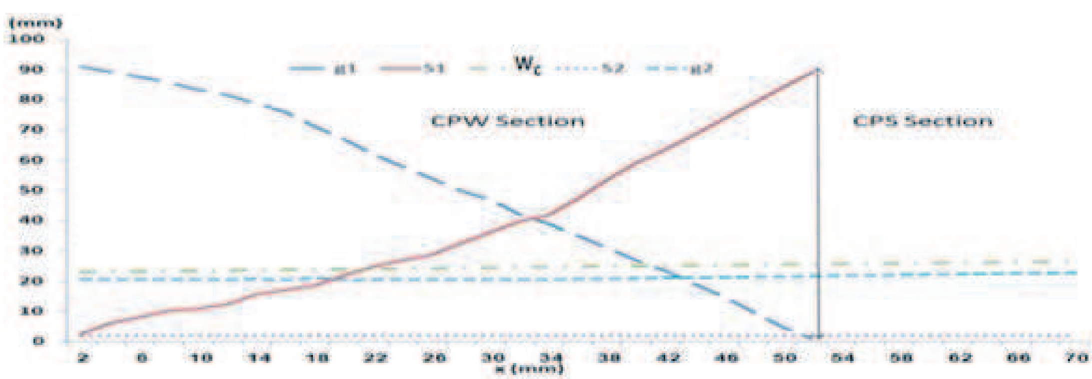

Figure 11. The changes of CPW-CPS transition parameters against transition length.

50 ohm to 80 ohm for the CPW section is only 52 mm for the exponential feeder which is smaller than the linear tapered feeder, so size reduction is achieved.

Designing the asymmetric CPW feeder shown in Fig. 9 is done by assuming the taper with the following equation:

$$Y = C_o * e^{K_o * X^2} \tag{2}$$

where C_o is the distance from the center line of the slot to the outer tapered slot line $C_o = W_c + S_1/2$, and K_o determines the rate of the exponential taper.

The transition is simulated in CST environment, and a parametric study is done on W_c, S_1, S_2, and K_o as shown in Figs. 12–15. For each step of the process, typical starting values are given from Table 2.

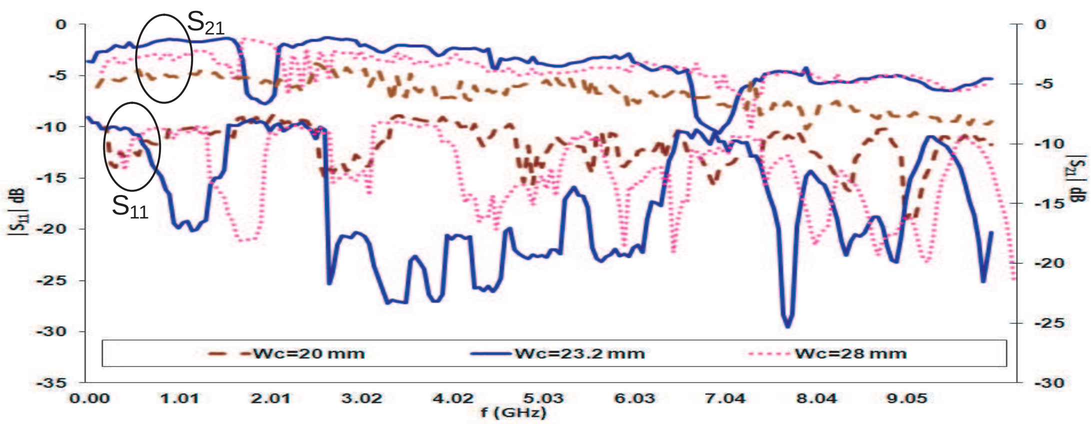

Figure 12. The changes of S_{11}, S_{21} for different values of W_c against frequency.

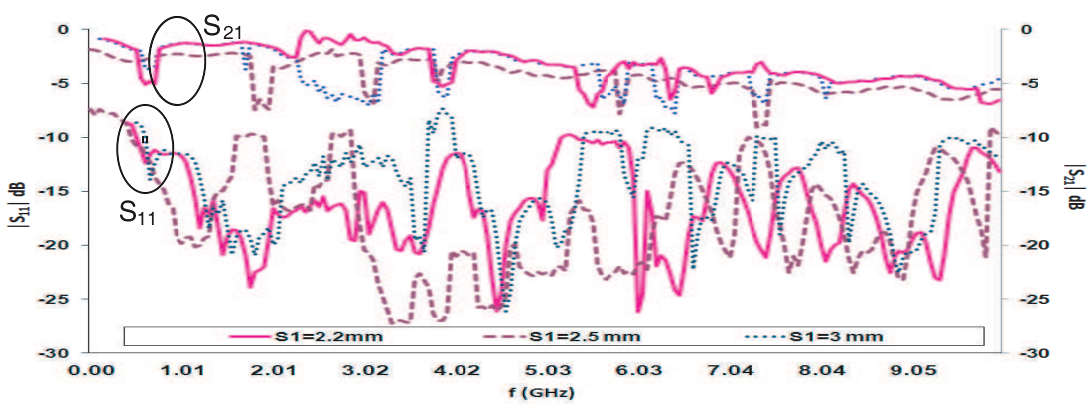

Figure 13. The changes of S_{11}, S_{21} for different values of S_1 against frequency.

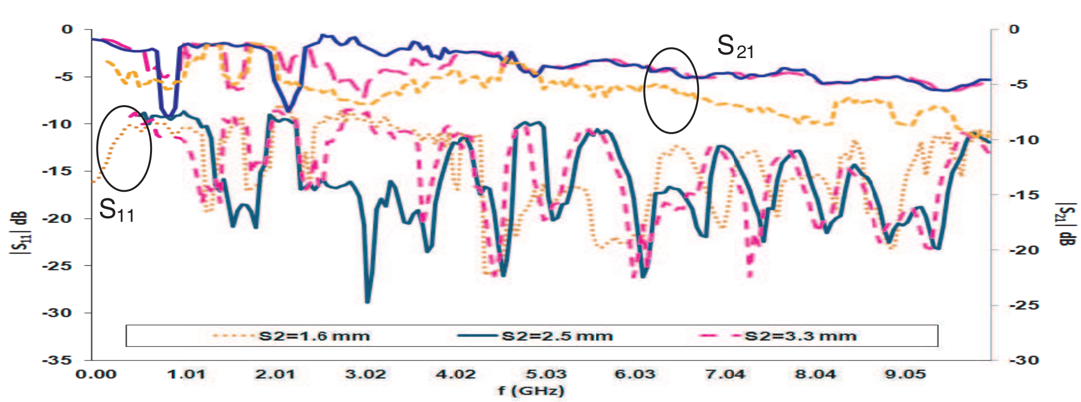

Figure 14. The changes of S_{11}, S_{21} for different values of S_2 against frequency.

As W_c increases, the insertion loss is improved; the bandwidth is enhanced from 0.5 GHz to 3 GHz; the optimum value of W_c is 23.2 mm as shown in Fig. 12. Also the optimum values of S_1 and S_2 are 2.2 mm and 2.5 mm, respectively, as shown in Figs. 13 and 14. As K_o changes, the bandwidth is changed until the optimum value for K_o is achieved at 0.03. The operating bandwidth becomes 8.4 GHz, and the insertion loss is decreased and becomes -2 dB as shown in Fig. 15. The optimum values of g_1 and g_2 are 91.2 mm and 20.8 mm, respectively.

For the remaining parameters R_1, R_2, initial values are assumed such that R_1 takes the values between 0 and L. According to the geometry of the antenna, assume $R_1 = 30$ mm, $L_{th} = 44$ mm and $R_2 \geq 1.5 * R_1$ to avoid any kind of reflection or coupling with the antenna radiating element.

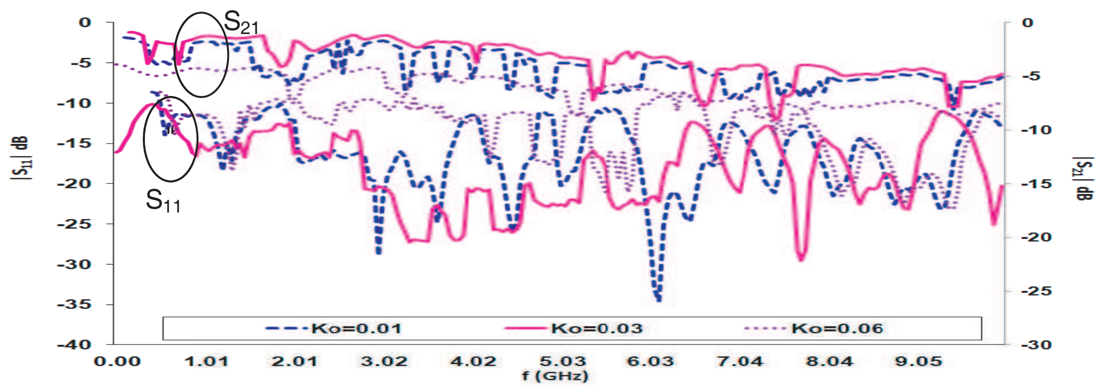

Figure 15. The changes of S_{11}, S_{21} for different values of K_o against frequency.

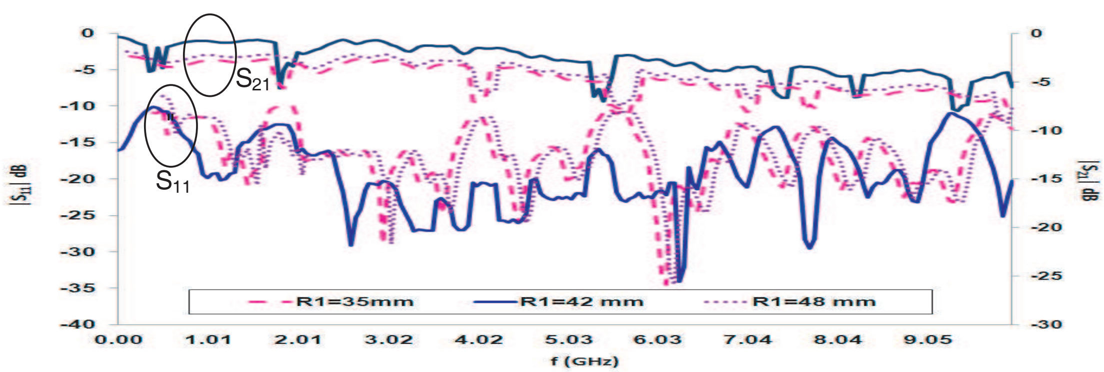

Figure 16. The changes of S_{11}, S_{21} for different values of R_1 against frequency ($R_2 = 75$ mm).

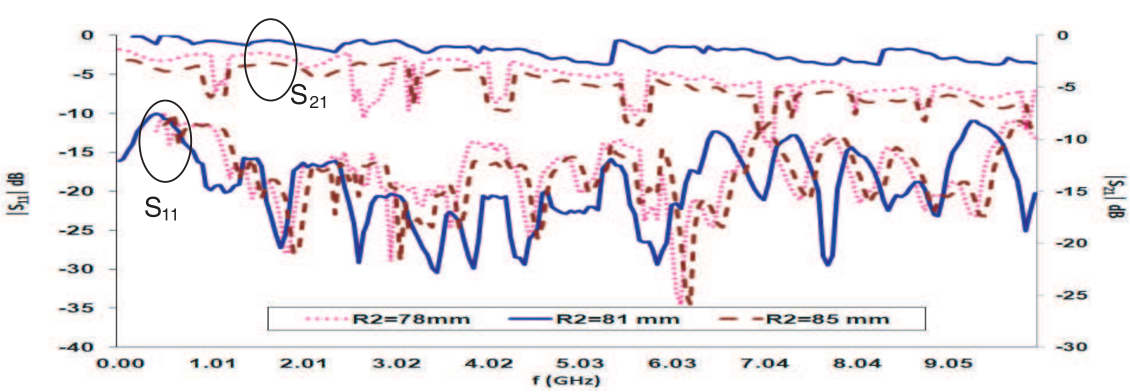

Figure 17. The changes of S_{11}, S_{21} for different values of R_2 against frequency ($R_1 = 42$ mm).

The selection of the circular shape for the CPW part not selecting exponential rate is due to the need to achieve fast matching within a limited area of extension, so size reduction is achieved.

The CPW to CPS transition shown in Fig. 9 is simulated using CST ver. 15, with the two transitions connected back to back. The size of the model is 140×140 mm. For the CPW, the dimensions $g_1 = 90$ mm, $S_1 = 2.2$ mm and $S_2 = 2.5$ mm. For the two parts of the strip line, one is connected to the CPW ground, and the other is connected to the CPW central conductor. All the dimensions are optimized to obtain the characteristic impedance of 50 ohm.

Figures 16 and 17 show the parametric studies of R_1 and R_2 when simulating the CPW to CPS back to back transition. As R_1 increases, the bandwidth is decreased, and the optimum value is $R_1 = 42$ mm. Also for R_2 the change is slightly small as it increases the lower frequency of the antenna and the optimum value of $R_2 = 81$ mm.

3.4. Effect of Circular Patches (Capacitive Loading) on the Return Loss and Insertion Losses

Figure 1 shows the back to back CPW-CPS transition with the capacitive loading "circular patches", which have shapes of circular patches aligned with the CPW section. Adding these patches slightly decreases the characteristic impedance of the CPW, as shown in Fig. 18. It also widens the bandwidth (S_{11} less than -10 dB), decreases the return loss and reduces the insertion losses as shown in Fig. 19, which shows the back to back CPW-CPS transition with and without the circular patches. The modifications summery can be described in Table 3.

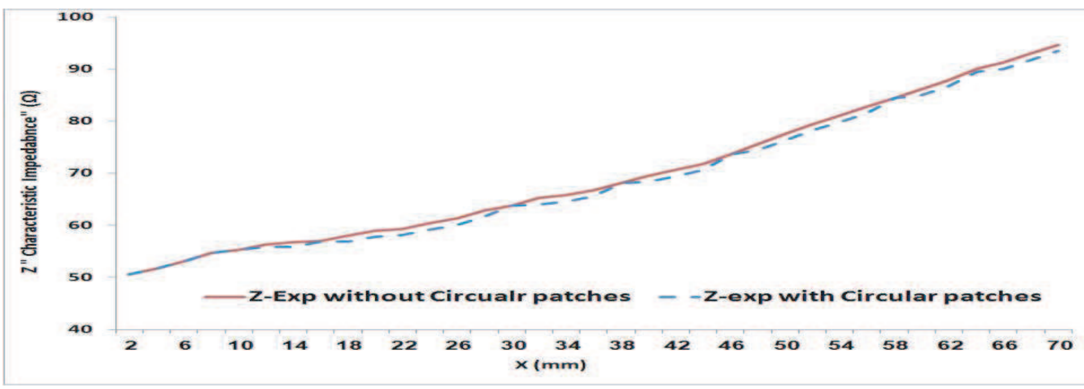

Figure 18. The effect of the circular patches on the characteristic impedance of the transition.

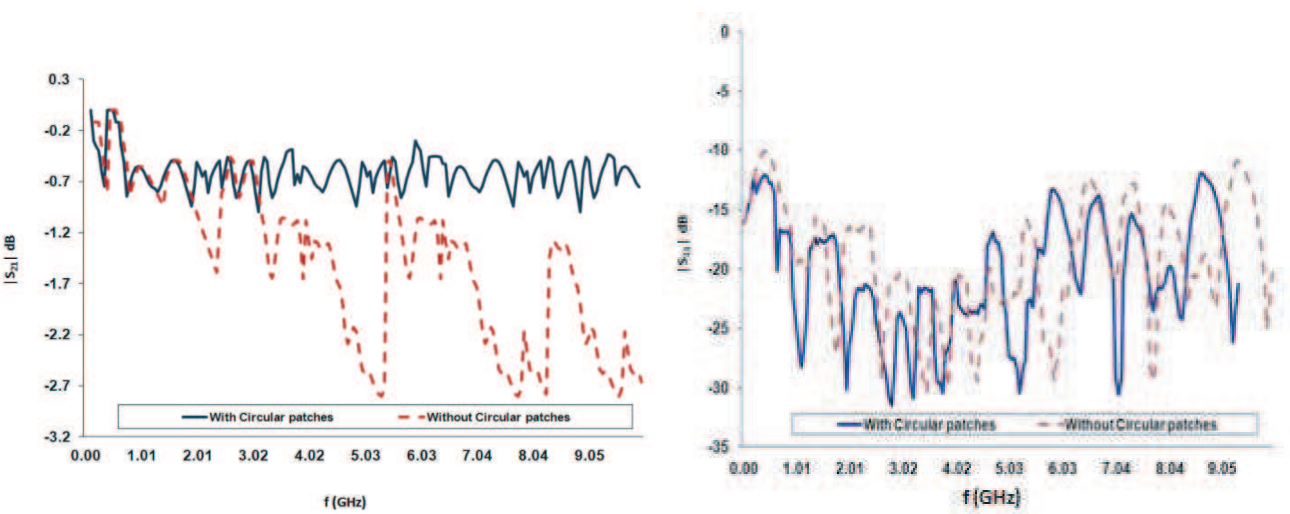

Figure 19. The S-parameters S_{11}, S_{21} with and without the circular patches.

Table 3. The modification steps for the proposed transition and the modeling parameters.

Item	Bandwidth (GHz)	Operating Frequency (GHz)	S_{21} (dB)
Designing Asymmetric CPW-CPS transition of linear tapered profile	1.5 GHz	1–2.5 GHz	4 dB
Designing Asymmetric CPW-CPS transition of exponential tapered profile	8.4 GHz	0.6–9 GHz	2 dB
Adding Circular patches effect	10 GHz	0–10 GHz	−0.45 dB

4. CPW TO CPS TRANSITION EQUIVALENT CIRCUIT MODELING

Designing the CPW to CPS transition is very complicated, due to the lack of a proven design procedure of adjustable parameters. This leads to the development of the analysis methodology and equivalent circuit model detailed below. The proposed equivalent circuit serves as a guide to validate the proposed design and understand the behavior of CPW-CPS transition shown in Fig. 1.

For the total CPW-CPS transition $L_{\text{CPW}} = 52\,\text{mm}$ and $L_{\text{CPS}} = 18\,\text{mm}$, the equivalent circuit model will be obtained using the following steps:

1. Divide the CPW section into 26 sub-sections with 2 mm sub-section length such that the geometric parameters g_1, g_2, S_1, S_2 and W_c may be considered constant in every sub-section, i.e., it can be described as uniform asymmetric CPW with different ground widths. Then calculate the characteristic impedance for the uniform ACPW sub-section as mentioned in [10, 13], Fig. 20.

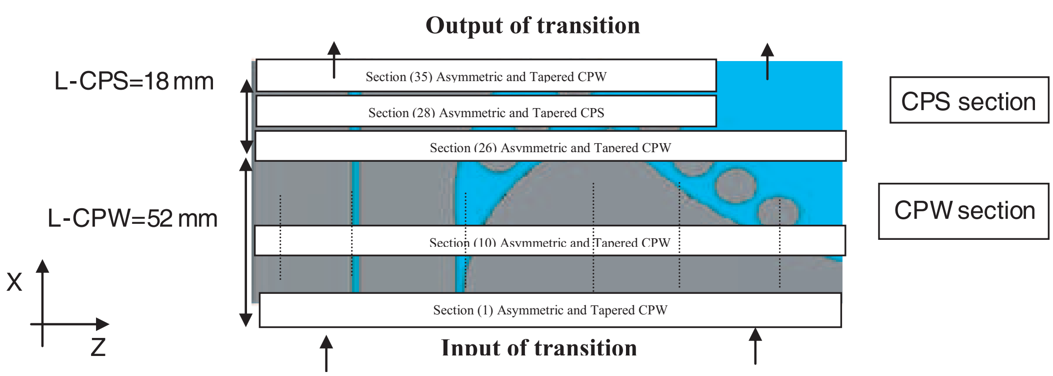

Figure 20. The proposed CPW to CPS transition sections.

2. Modify the characteristic impedance calculated in step 1, by calculating the characteristic impedance using the method mentioned in [8, 9] for nonuniform CPW section.
3. Repeat steps (1) and (2) to calculate the characteristic impedance for CPS section [10], and note that the number of sections is 9.
4. Calculate $ABCD$ parameters for each section.
5. Calculate the total $ABCD$ parameters for the 35 sections using a MATLAB program.
6. Construct and calculate the back to back transition $ABCD$ parameters.
7. Transform $ABCD$ parameters to S-parameters.
8. Compare the calculated S-parameters (Equivalent Circuit model) and the simulated one (CST ver. 15) to verify the results.

Figure 20 shows the proposed CPW-CPS transition sections classification, and the $ABCD$ equivalent circuit model is shown in Fig. 21.

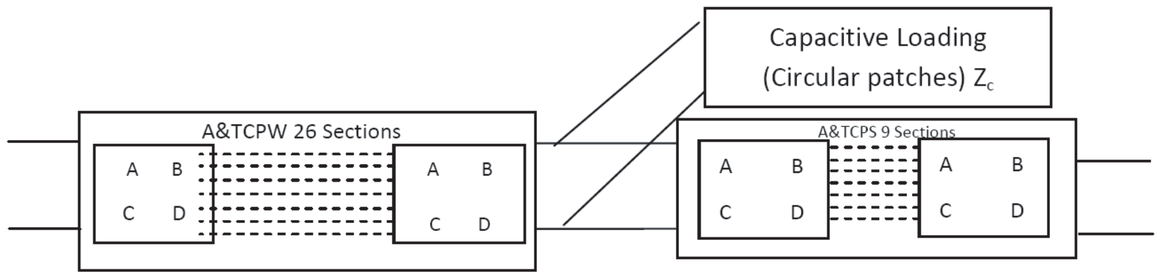

Figure 21. Equivalent circuit model.

4.1. Modification of Characteristic Impedance Calculation and $ABCD$ Parameters

For theoretical analysis, each nonuniform transmission line is divided into sections. In each section, the characteristic impedance varies linearly, and the propagation constant is assumed to be constant. Let the characteristic impedance profile in the nth section starts with Z_o and varies linearly with slope along the length. The two-port $ABCD$ matrix elements of the nth section can then be given by [8, 9].

The modified characteristic impedance and propagation coefficient for the nonuniform section shown in Figs. 22(a), (b) for both CPW and CPS section are [8, 9]:

$$Z_C(x) = Z_c(0)(1+kx) \tag{3}$$

$$\beta_o = \frac{\omega}{c} \tag{4}$$

where x is the position along the line, k the slope constant, L the length of the line ($L = 2\,\text{mm}$), ω the angular frequency, c the velocity of the light, $Z_c(0)$ the uniform characteristic impedance for every section which is calculated for both CPW and CPS sections from [10, 13] respectively and also shown in Fig. 10.

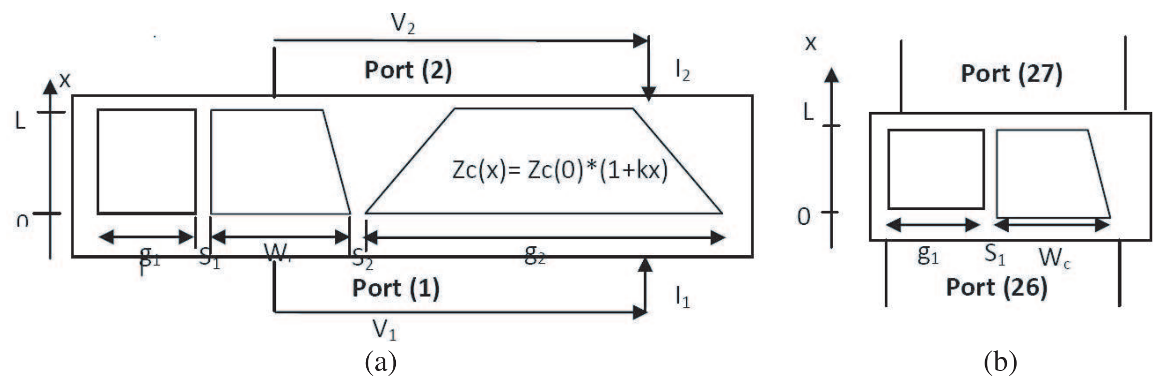

Figure 22. (a) The CPW section. (b) The CPS section.

The generalized telegraph equation describing this system can be written as:

$$\frac{d^2V(x)}{dx^2} - \frac{k}{1+kx}\frac{dV(x)}{dx} + \beta_0^2 V(x) = 0 \tag{5}$$

$$\frac{d^2I(x)}{dx^2} + \frac{k}{1+kx}\frac{dI(x)}{dx} + \beta_0^2 I(x) = 0 \tag{6}$$

It is found that the solution of this equation is

$$V(x) = (1+kx)\left\{K_1 J_1\left[\frac{\beta_0}{k}(1+kx)\right] + K_2 Y_1\left[\frac{\beta_0}{k}(1+kx)\right]\right\} \tag{7}$$

$$I(x) = -\frac{1}{Z_c}\frac{dV(x)}{dx} = \frac{1}{Z_c}\left(\frac{C_1 k}{\beta_0}\left[\frac{\beta_0}{k}(1+kx)J_0\left(\frac{\beta_0}{k}(1+kx)\right)\right] + \frac{C_2 k}{\beta_0}\left[\frac{\beta_0}{k}(1+kx)Y_0\left(\frac{\beta_0}{k}(1+kx)\right)\right]\right)\beta_0 \quad (8)$$

where J_0 and J_1 are the Bessel functions of the first kind of orders 0 and 1, respectively. Y_o and Y_1 are the Bessel function of second kind of orders 0 and 1, respectively.

Let $r = \frac{\beta_0}{k}(1+kx)$, at $x = 0$ $r_1 = \frac{\beta_0}{k}$ and at $x = L$ $r_2 = \frac{\beta_0}{k}(1+kL)$.

We can now write:

At $x = 0$

$$V_1(0) = \{C_1 J_1[r_1] + C_2 Y_1[r_1]\} \quad (9)$$

$$I_1(0) = -\frac{k}{z_c}(C_1[J_0(r_1)] + C_2[Y_0(r_1)]) \quad (10)$$

At $X = L$

$$V_2(L) = r_2\frac{k}{\beta_0}\{C_1 J_1(r_2) + C_2 Y_1(r_2)\} \quad (11)$$

$$I_2(L) = -\frac{kr_2}{z_c}(C_1[J_0(r_2)] + C_2[Y_0(r_2)]) \quad (12)$$

Now we can derive expressions for $ABCD$ parameters as follows:

$$\begin{bmatrix} V_1 \\ I_1 \end{bmatrix} = \begin{bmatrix} A & B \\ C & D \end{bmatrix}\begin{bmatrix} V_2 \\ I_2 \end{bmatrix}$$

$$A = \frac{\{Y_0(r_2)J_1[r_1] - J_0(r_2)Y_1[r_1]\}}{r_2\frac{k}{\beta_0}\{Y_0(r_2)J_1(r_2) - J_0(r_2)Y_1(r_2)\}} \quad (13)$$

$$B = \frac{Z_{c2}(Y_1(r_2)\{J_1[r_1] - J_1(r_2 Y_1[r_1]\})}{-kr_2(Y_1(r_2)[J_0(r_2)] - J_1(r_2)[Y_0(r_2)])} \quad (14)$$

$$C = \frac{-\beta_0(Y_0(r_2)[J_0(r_1)] - J_0(r_2)[Y_0(r_1)])}{Z_{c1}r_2\{Y_0(r_2)J_1(r_2) - J_0(r_2)Y_1(r_2)\}} \quad (15)$$

$$D = \frac{Z_{c2}(Y_1(r_2)[J_0(r_1)] - J_1(r_2)[Y_0(r_1)])}{Z_{c1}r_2(Y_1(r_2)[J_0(r_2)] - J_1(r_2)[Y_0(r_2)])} \quad (16)$$

The calculated $ABCD$ parameters for this model are different from the $ABCD$ parameters mentioned in [8, 9] as the published papers assume that the $ABCD$ matrix for every section is obtained by applying proper boundary conditions, but here the $ABCD$ matrix is solved in general form to obtain an accurate solution.

From Fig. 21, the total $ABCD$ matrix for CPW-CPS back to back transition will include the $ABCD$ matrices of total sections of ACPW and ACPS, and can be evaluated by cascading the matrices for all nth sections, where $n = 70$ sections, i.e., for the CPW-CPS back to back transition, and also the $ABCD$ matrix for capacitive loading (circular patches).

$$\begin{bmatrix} A^t & B^t \\ C^t & D^t \end{bmatrix} = \prod_{n=1}^{70}\begin{bmatrix} A_i & B_i \\ C_i & D_i \end{bmatrix}$$

$$= \prod \begin{bmatrix} A^t_{cpw(1-10)} & B^t_{cpw(1-10)} \\ C^t_{cpw(1-10)} & D^t_{cpw(1-10)} \end{bmatrix}\begin{bmatrix} 1 & 0 \\ \frac{1}{Z_{c(11-26)}} & 1 \end{bmatrix}\begin{bmatrix} A^t_{cpw(11-26)} & B^t_{cpw(11-26)} \\ C^t_{cpw(11-26)} & D^t_{cpw(11-26)} \end{bmatrix}\begin{bmatrix} 1 & 0 \\ \frac{1}{Z_{c(27-35)}} & 1 \end{bmatrix}$$

$$\begin{bmatrix} A^t_{cps(27-35)} & B^t_{cps(27-35)} \\ C^t_{cps(27-35)} & D^t_{cps(27-35)} \end{bmatrix}\begin{bmatrix} 1 & 0 \\ \frac{1}{Z_{c(36-44)}} & 1 \end{bmatrix}\begin{bmatrix} A^t_{cps(36-44)} & B^t_{cps(36-44)} \\ C^t_{cps(36-44)} & D^t_{cps(36-44)} \end{bmatrix}\begin{bmatrix} 1 & 0 \\ \frac{1}{Z_{c(45-60)}} & 1 \end{bmatrix}$$

$$\begin{bmatrix} A^t_{cpw(45-60)} & B^t_{cpw(45-60)} \\ C^t_{cpw(45-60)} & D^t_{cpw(45-60)} \end{bmatrix}\begin{bmatrix} A^t_{cpw(61-70)} & B^t_{cpw(61-70)} \\ C^t_{cpw(61-70)} & D^t_{cpw(61-70)} \end{bmatrix} \quad (17)$$

The capacitive loading increases the bandwidth and decreases the insertion losses of the transition.

$$Z_{cn} = \frac{1}{j\omega C_n} \tag{18}$$

where ω is the angular frequency, and C_n is the sub-section capacitance of the circular patches, as shown in Fig. 23 the sample of the circular patch and the right-hand side of the CPW section.

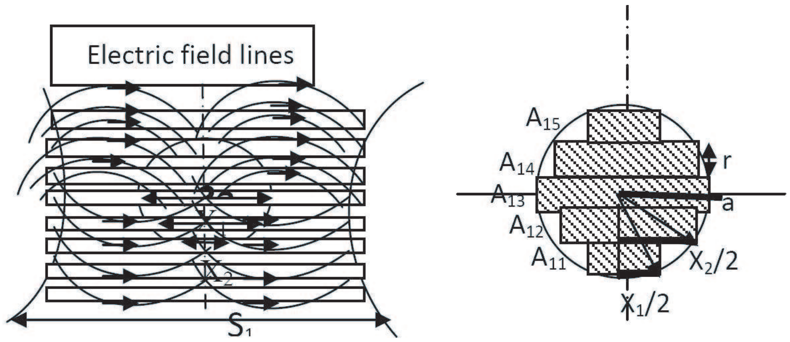

Figure 23. The sample of the circular patch and the electric field lines.

Due to the small distances between the circular patches and CPW or CPS sections, it will be assumed as an appropriate approximation that the circular patches will act as equivalent parallel plate capacitors with average electric field lines E_{avg} and lengths d_{avg} and with effective permittivity ε_{eff}, i.e., assume a constant intensity of electric field lines and constant potential difference between adjacent conductors. Note that all of the above assumption is proposed and verified later with the CST simulation, and good results are obtained. So the capacitance will be as follows:

$$C_n\text{— for each section} = \frac{\varepsilon_o \varepsilon_{eff} A_n}{d_{avg}} \quad C_n = 0 \text{ for } n = 1:10 \text{ and also for } n = 60:70 \tag{19}$$

where A_n is the area of the patch part in each section, and the section width is $r = 2\,\text{mm}$. Also as shown in Fig. 23, we take a section as an example to show how the capacitance is calculated, and this procedure will be repeated for all sections.

So, $A_{11} = A_{15} = X_1 * r = 2\sqrt{(}a^2 - (2.5r)^2) * r$, $A_{12} = A_{14} = X_2 * r = 2\sqrt{(}a^2 - (1.5r)^2) * r$, $A_{13} = 2a * r$, $d_{avg} = \pi\frac{S_1}{2}$, $\varepsilon_{eff} = \frac{(\varepsilon_r+1)}{2}$ where $\varepsilon_r = 4.65$ (FR4 substrate).

The capacitance will be calculated for all sections in $n = 11:60$ sections for the CPW-CPS back to back transition. After obtaining the $ABCD$ matrix using Eqs. (17) and (18), the input impedance for the total transition can be given by:

$$Z_{in} = \frac{A^t Z_L + B^t}{C^t Z_L + D^t} \tag{20}$$

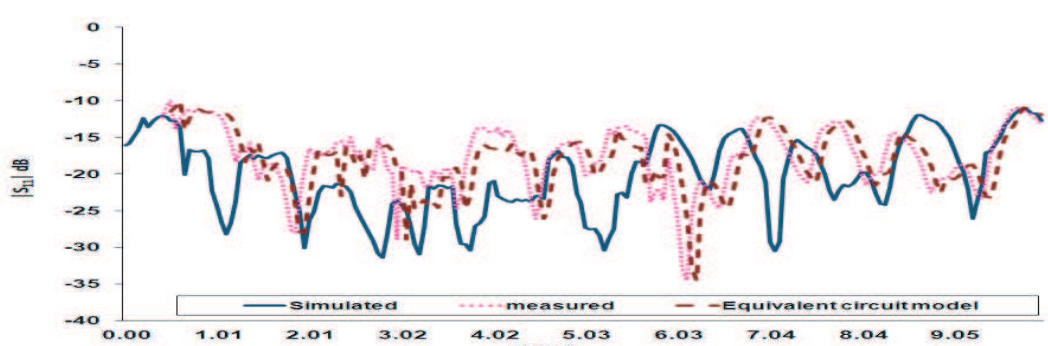

Figure 24. $|S_{11}|$ of back to back CPW to CPS transition configuration based on equivalent circuit model, CST simulation and measurements.

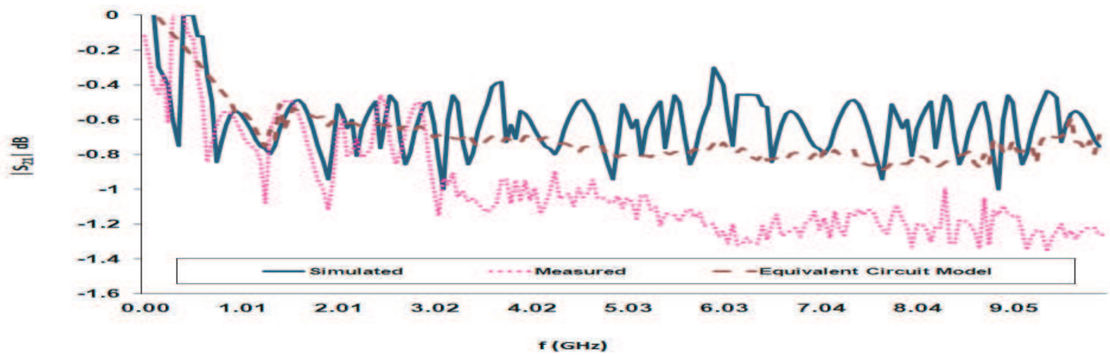

Figure 25. $|S_{21}|$ of back to back CPW to CPS transition configuration based on equivalent circuit model, CST simulation and measurements.

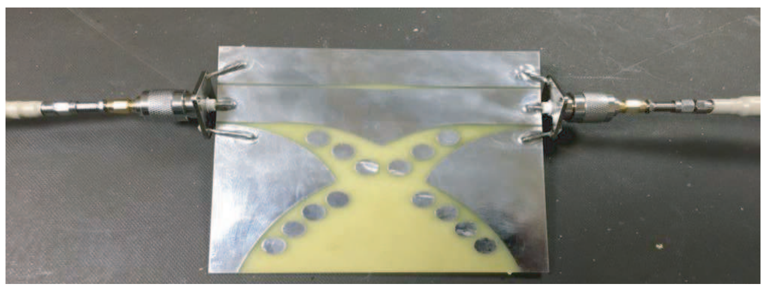

Figure 26. A photo for the fabricated CPW to CPS back to back transition.

where $Z_L = 50\,\Omega$ for the Back to Back transition.

All of the $ABCD$ parameters calculation is done using MATALB program. By calculating the Z_{in} using Eq. (20), the total S-parameters based on the equivalent circuit model can be calculated. The back to back CPW-CPS transition has been fabricated, and the S-parameters have been measured. Comparisons among calculated S-parameters based on equivalent circuit model, simulated S-parameters based on the CST simulation, and measured S-parameters are shown in Fig. 24 and Fig. 25. There is a good agreement between simulated and measured results. The small discrepancy between them, especially for the GPR ranges of frequencies, may be attributed to fabrication tolerances and launcher soldering. A photo for the fabricated back to back CPW-CPS transition is shown in Fig. 26.

5. CONCLUSION

A novel ultra-wideband CPW to CPS transition for TSA in landmine detection using GPR system is proposed. It is composed of 2 sections. The first is nonuniform tapered asymmetric coplanar waveguide (TACPW), and the second consists of nonuniform tapered asymmetric coplanar strips (TACPS). An EBG structure of coplanar circular patches exists near the transition open slot and aligned with the outer edge of the CPW ground. The CPW to CPS transition is analyzed theoretically and experimentally. Equivalent-circuit model that consists of nonuniform transmission lines is established. The equivalent circuit is constructed by dividing both sections TACPW and TACPS into 35 sub-sections and using $ABCD$ parameters to characterize each section, and conversion to S-parameters is done. MATLAB Program is used for $ABCD$ parameters calculations and the conversion to S-parameters. The design verification is done by comparing the calculated and converted S parameters and simulated one using CST studio simulation (Ver. 15). The results based on equivalent-circuit model, CST simulation and measurements are compared. The operational bandwidth for the CPW to CPS transition covers from 0 (DC) to almost 10 GHz with minimum return loss reaching -50 dB. For the GPR application (landmine detection) which extends from 0.4 to 3 GHz, the insertion loss of the proposed transition reaches almost -0.5 dB which satisfies the design requirements. The back to back transition performance is simulated and measured. Good agreement is found between numerical and experimental results especially for the GPR ranges of frequencies.

REFERENCES

1. Sturdivant, R., *Microwave and Millimeter-wave Electronic Packaging*, 1st Edition, Artech House, USA, 2014.
2. Zhang, F., G. Y. Fang, Y. J. Ju, and J.-J. Shao, "A novel compact double exponentially tapered slot antenna (DETSA) for GPR applications," *IEEE Trans. Antennas Propag.*, Vol. 11, No. 1, 195–198, 2011.
3. Huang, C. H., T. S. Horng, C. C. Wang, C. T. Chiu, and C. P. Hung, "Optimum design of transformer-type Marchand balun using scalable integrated passive device technology," *IEEE Trans. on Components, Packaging and Manufacturing Technology*, Vol. 2, No. 8, 1370–1377, 2012.
4. Ma, R. and J. Fu, "Microstrip to coplanar strip double-Y balun with very high upper frequency limitation," *3rd Asia-Pacific Conference on Antennas and Propag. (APCAP)*, China, 2014.
5. Butrym, A. and S. Pivnenko, "CPW to CPS transition for feeding UWB antennas," *2nd International Workshop Ultrawideband and Ultrashort Impulse Signals*, Ukraine, 2004.
6. Anagnostou, D. E., M. Morton, J. Papapolymerou, and G. Christodoulou, "A 0–55-GHz coplanar waveguide to coplanar strip transition," *IEEE Trans. on Microwave Theory and Techniques*, Vol. 56, No. 1, 1–6, 2008.
7. Zhu, L., "Periodically loaded transmission line media/materials with infinite extent on coplanar waveguide: Guided-wave performances," *Proceedings of Asia-Pacific Microwave Conference*, China, 2006.
8. Mao, S. G., C. T. Hwang, R. B. Wu, and C. H. Chen, "Analysis of coplanar waveguide-to-coplanar Stripline transitions," *IEEE Trans. on Microwave Theory and Techniques*, Vol. 48, No. 1, 23–29, 2001.
9. Lu, K., "An efficient method for analysis of arbitrary non-uniform transmission lines," *IEEE Trans. on Microwave Theory and Techniques*, Vol. 45, No. 1, 9–14, 1997.
10. Garg, R., I. Bahl, and M. Bozzi, *Microstrip Lines and Slot Lines*, 3rd Edition, Artech House, USA, 2013.
11. Omar, S. A., A. Iqbal, O. A. Saraereh, and A. Basir, "An array of M-shaped vivaldi antennas for UWB applications," *Progress In Electromagnetics Research Letters*, Vol. 68, No. 9, 67–72, 2017.
12. Fei, P., Y.-C. Jiao, Y. Ding, and F.-S. Zhang, "A compact coplanar waveguide fed wide tapered slot ultra-wideband antenna," *Progress In Electromagnetics Research Letters*, Vol. 25, 77–85, 2011.
13. Duyar, M., V. Akan, E. Yazgan, and M. Bayrak, "Analytical attenuation calculation of asymmetrical coplanar waveguide with finite extent ground planes for coplanar waveguide mode," *Microwave and Optical Technology Letters*, Vol. 49, No. 9, 2082, 2087, September 2007.
14. Abuhalima, S., E. Abdallah, and D. Mohamed, "Ultra wideband elliptical microstrip antenna using different taper lines for feeding," *11th WSEAS International Conference on Communications*, 144–149, Greece, July 26–28, 2007.